Exotic meson decay widths using lattice QCD

M. S. Cook[*] and H. R. Fiebig[†]

Department of Physics, Florida International University, Miami, Florida, USA 33199
(Received 5 June 2006; published 15 August 2006)

A decay width calculation for a hybrid exotic meson h, with $J^{PC} = 1^{-+}$, is presented for the channel $h \to \pi a_1$. This quenched lattice QCD simulation employs Lüscher's finite box method. Operators coupling to the h and πa_1 states are used at various levels of smearing and fuzzing, and at four quark masses. Eigenvalues of the corresponding correlation matrices yield energy spectra that determine scattering phase shifts for a discrete set of relative πa_1 momenta. Although the phase shift data is sparse, fits to a Breit-Wigner model are attempted, resulting in a decay width of about 60 MeV when averaged over two lattice sizes having a lattice spacing of 0.07 fm.

I. INTRODUCTION

Hybrid mesons are quark-antiquark pairs having valence gluons as a structural component. In some cases their quantum numbers are not accessible with quark models, and they are therefore called exotic. Examples of these exotics are the $J^{PC} = 0^{+-}$, 1^{-+}, and 2^{+-} mesons. Because these mesons contain valence gluons their verification is one of the signature tests of quantum chromodynamics (QCD).

Efforts to determine properties of these hybrid exotic states are unsettled from both experimental and theoretical viewpoints [1–3]. The experimental efforts date back over a decade [4–10], and currently, considerable resources are being devoted to their future study. The Jefferson Lab GlueX experimental program is designed to investigate exotic states. Hybrid meson studies are also part of the COMPASS experiment at CERN and the CLEOc program at Cornell.

Attempts to calculate decay widths of hybrid mesons have been made using the bag model [11], the quark model extended by gluon flux tube degrees of freedom [12,13] and in lattice QCD [14,15].

Calculating properties of resonances using Euclidean lattice QCD simulations is not straightforward for a variety of reasons. On a finite lattice all states are bound, and furthermore, the lattice total energy of a two-hadron state in a decay channel is typically larger than the energy of the original hadron thus preventing decay. Aspects of these points have been discussed by Michael [16,17], DeGrand [18], Lüscher [19], and by Lellouch and Lüscher [20].

Thus, lattice work on hybrid mesons has concentrated mainly on their mass spectrum. It can be roughly classified in terms of heavy quark systems using static quarks with (excited) glue treated in the Born-Oppenheimer approximation [21–23], using nonrelativistic QCD [24–26], and studies using actions with both quenched and unquenched quark dynamics [27–34]. Lattice work on hadron reso-

nances, of which there is very little at this time, has recently been reviewed by Michael [17].

Hybrid meson decay widths have been studied on the lattice in the heavy quark limit [15] and, recently, for light quarks [14]. In those studies the time dependence (slope) of a normalized transition matrix element computed on the lattice is related to a decay width via Fermi's golden rule [35]. For this approach to work the lattice parameters have to be such that the resonance mass comes out close to the threshhold of the decay channel.

We here choose to extract decay widths using Lüscher's finite box method [19,36,37]. In principle, Lüscher's method is rigorous: The two-particle energy spectrum in a finite periodic box is related to continuum elastic scattering amplitudes. The spectra allow calculation of the scattering phase shifts at a discrete set of momenta owing to exact formulas derived by Lüscher. A decay width can then be extracted by fitting a Breit-Wigner function, provided a resonant state is actually present. The applicability of this method to extract scattering phase shifts has been demonstrated for the O(3) nonlinear sigma model in $1 + 1$ dimensions [38], the O(4) nonlinear sigma model in $3 + 1$ dimensions [39,40], meson-meson scattering in $2 + 1$ dimensions using QED [41], and resonance scattering of two coupled Ising systems [42,43].

Application of Lüscher's method to our desired goal requires a set of operators that couple to the hybrid meson state and to appropriate two-meson systems matching a decay channel. The exotic 1^{-+} meson can decay into πb_1, πf_1, and πa_1, which are relative S-wave channels. Other decays are possible, but those involve relative P-waves, where the relative momentum is at least $2\pi/L$, and thus give rise to large upward energy shifts which makes the simulation more difficult [18,35,44]. We note that experimentally [45] the three mesons $b_1(1235)$, $a_1(1260)$, $f_1(1285)$ are close in mass, and that the a_1 is a vector meson with $C = +$ so that it combines naturally with $C = 0$ of the (neutral) pion to the required charge conjugation, $C = +$, of the exotic meson. Therefore, in this study, we model our two-hadron operator after the πa_1 decay channel.

---
[*]Electronic address: mcook003@fiu.edu
[†]Electronic address: fiebig@fiu.edu

II. LATTICE PARAMETERS

Obtaining excited state spectra from correlation matrices that involve two-hadron operators presents a numerical challenge in itself. On top of this more analysis steps are required to obtain a decay width, which essentially amounts to extracting a "derivative" quantity from the simulation. While statistical errors, and also discretization errors to some extent, can be easily controlled this is not true for the systematic uncertainties indigenous to a task of this kind. For this reason we have refrained from using large computing resources and therefore employed a very simple lattice action and moderate lattice sizes and pion masses.

Simulations were performed using the Wilson gauge field action and Wilson fermions in quenched approximation on anisotropic lattices. We will present results from 200 gauge configurations on $12^3 \times 24$ and $10^3 \times 24$ lattices.

The definition of the coupling parameters used for the Wilson gauge action

$$S_g[U] = \sum_x \sum_{1 \le \mu < \nu \le 4} \beta_{\mu\nu} \left(1 - \tfrac{1}{3} \mathrm{Re}\,\mathrm{Tr}(U_{\mu\nu}(x))\right) \qquad (1)$$

is given by

$$\beta_{\mu\nu} = \beta \frac{a_1 a_2 a_3 a_4}{(a_\mu a_\nu)^2}, \qquad (2)$$

where $\mu\nu$ denotes plaquette planes and $a_1 = a_2 = a_3 =: a_s$ is the spatial and $a_4 =: a_t$ the temporal lattice constant. We have chosen the (bare) anisotropy $\xi = a_s/a_t = 2$ and $\beta = 6.15$ for the global coupling parameter. Parameters for the anisotropic fermion matrix

$$Q(x, y) = \mathbf{1}\delta_{x,y} - \sum_\mu \kappa_\mu \Big((1 - \gamma_\mu)U_\mu(x)\delta_{x+\hat{\mu},y}$$
$$+ (1 + \gamma_\mu)U_\mu^\dagger(y)\delta_{x,y+\hat{\mu}}\Big), \qquad (3)$$

are given by

$$\kappa_\mu = \kappa \frac{4}{a_\mu \sum_\lambda \frac{1}{a_\lambda}}, \qquad (4)$$

where κ is a global hopping parameter. With these conventions the relation of the latter to the (bare) Wilson quark mass parameter m_q is

$$\kappa = \frac{\sum_\lambda \frac{1}{a_\lambda}}{8(m_q + \sum_\lambda \frac{1}{a_\lambda})}, \qquad (5)$$

which identifies $\kappa_c = 0.125$ as the critical value.

Correlation functions for mesons from standard local operators $\pi \sim \gamma_5$, $\rho \sim \gamma_i$, and $a_1 \sim \gamma_i\gamma_5$, $i = 1, 2, 3$ were constructed as a matter of course employing three iterations of quark field smearing [46] and gauge field

fuzzing [47]. Also, within this setting, we adopted the hybrid meson operator proposed in [48] with magnetic type gluons

$$O_h(t) = \sum_{1 \le i < j \le 3} \sum_{\vec{x}} \bar{d}_a(\vec{x}t)\gamma_i u_b(\vec{x}t)[F_{ij}^{ab}(\vec{x}t) - F_{ij}^{\dagger ab}(\vec{x}t)], \qquad (6)$$

where a, b denote color indices and $F_{ij}(x)$ is a product of SU(3) link matrices arranged in a clover pattern

$$F_{\mu\nu}(x) = U_\mu(x)U_\nu(x + \hat{\mu})U_\mu^\dagger(x + \hat{\nu})U_\nu^\dagger(x)$$
$$+ U_\nu(x)U_\mu^\dagger(x - \hat{\mu} + \hat{\nu})U_\nu^\dagger(x - \hat{\mu})U_\mu(x - \hat{\mu})$$
$$+ U_\mu^\dagger(x - \hat{\mu})U_\nu^\dagger(x - \hat{\mu} - \hat{\nu})U_\mu(x - \hat{\mu} - \hat{\nu})$$
$$\times U_\nu(x - \hat{\nu}) + U_\nu^\dagger(x - \hat{\nu})U_\mu(x - \hat{\nu})$$
$$\times U_\nu(x + \hat{\mu} - \hat{\nu})U_\mu^\dagger(x), \qquad (7)$$

which is used in the spatial planes only. Under parity we have $\mathcal{P}O_h(t)\mathcal{P}^{-1} = -O_h(t)$, while for the charge neutral ($\bar{d}u \to \bar{u}u, \bar{d}d$) version $O_{h^0}(t)$ of (6) under charge conjugation the derivation of $\mathcal{C}O_{h^0}(t)\mathcal{C}^{-1} = -O_{h^0}(t)$ relies on the presence of $F - F^\dagger$, specifically $\mathcal{C}F_{ij}(x)\mathcal{C}^{-1} = F_{ij}^*(x)$. We have enforced this relation in the simulation: Observing that $S_g[U] = S_g[U^*]$ the configurations $[U]$ and $[U^*]$ are equally probable. Thus with each $[U]$ in the ensemble of 200 configurations we also include $[U^*]$ and compute fermion propagators for both of those. This strategy doubles the number of fermion propagators that need to be computed, however, charge conjugation is now numerically exact, and this also appears to be the reason for an observed noise reduction of simulation signals.

Meson masses were obtained at four values of the hopping parameter κ, see Table I. A multiple mass inverter [49] was used to compute propagators. The resulting ground state masses, coming from three smearing iterations, sources set at $t = 3$, and effective mass function fits in the range $t = 6 \ldots 11$, are also listed in Table I.

In order to allow extrapolations to the small pion mass region it is useful to study the dependence of the computed ρ, a_1 and h masses on $M_\pi = a_t m_\pi$. Predictions for this

TABLE I. List of hopping parameters κ and the resulting π, ρ, a_1 and h meson masses in units of the temporal lattice constant a_t for lattices $12^3 \times 24$ (upper table) and $10^3 \times 24$ (lower table).

κ	$a_t m_\pi$	$a_t m_\rho$	$a_t m_{a_1}$	$a_t m_h$
0.140	0.53(4)	0.55(3)	0.65(4)	0.63(25)
0.136	0.64(3)	0.65(3)	0.75(3)	0.75(21)
0.132	0.75(3)	0.75(3)	0.86(3)	0.85(26)
0.128	0.85(4)	0.85(3)	0.96(3)	0.95(24)
0.140	0.54(5)	0.54(3)	0.64(4)	0.62(24)
0.136	0.65(3)	0.62(3)	0.75(3)	0.71(23)
0.132	0.74(3)	0.73(3)	0.85(4)	0.81(25)
0.128	0.85(4)	0.83(3)	0.96(3)	0.91(22)

dependence may in principle come from chiral perturbation theory [50], and will depend on the baryon being studied. For a baryon of mass $M = a_t m$ the expression

$$M \approx p_0 + p_2 M_\pi^2 + p_3 M_\pi^3 + p_4 M_\pi^4 + q M_\pi^4 \ln(M_\pi), \quad (8)$$

contains a collection of terms typical for χPT inspired models [51–53]. In the case of the hybrid exotic meson, for example, the authors of [54] retain only the even polynomial in (8). For the πa_1 decay channel, which is mostly relevant in this work, no predictions for the dependence of the spectral masses, say W, on M_π are available. A three parameter model that reflects features of (8) is

$$W = p + qx + r \ln(1 + x) \quad \text{with} \quad x = (a_t m_\pi)^2. \quad (9)$$

The logarithmic term is purely heuristic. Its role is to

provide curvature to the model, just like the last three terms in (8) do while vanishing as $M_\pi \to 0$. As it turns out this model yields fits that are on average optimal on our spectral data for the combined h and πa_1 systems. Replacing the logarithmic term in (9) with $x^{3/2}$ yields nearly identical results.

We consistently use (9) to fit all masses emerging from the simulation. Examples for the mesons listed in Table I are shown in Fig. 1.

In particular the upper panel of Fig. 1 exhibits a level crossing between the hybrid meson mass and the $\pi + a_1$ mass, assuming a relative S-wave for the latter. The level crossing emerges near $x \simeq 0$ which is only reached through extrapolation. The lower panel illustrates the effect of P-wave vs S-wave decay on the lattice. The mass of the $\pi + \pi$ system is shown with pions having lattice momenta $\pm 2\pi/(a_s L)$. Clearly a level crossing with the ρ meson mass is harder to achieve.

The extrapolated ρ meson mass, at $x = 0$, shall be used to set the physical mass or length scale for this simulation. We obtain $a_t = 0.33(5)$ GeV$^{-1} = 0.07(1)$ fm $(m_\rho = 776$ MeV). If the a_1 meson is used instead the scale is $a_t = 0.30(3)$ GeV$^{-1} = 0.06(1)$ fm $(m_{a_1} = 1230$ MeV). The above numbers are based on the $12^3 \times 24$ lattice. Unless otherwise indicated we will quote results using the ρ meson to set the scale.

As a sideline it is interesting to note that the level crossing seen in Fig. 1, using both of the above scales, thus occurs within 1.35–1.49 GeV, which overlaps with the experimental mass of the $\pi(1400)$ resonance, according to [45]. Indeed the $\pi(1400)$ has the quantum numbers 1^{-+} of the hybrid exotic meson. This observation coincides with the findings of [54].

III. CORRELATION MATRIX

The description of $h \to \pi + a_1$ requires an operator for the two-meson decay channel with suitable quantum numbers. Consider

$$O_{\pi^+ a_1^0; k, \vec{r}}(t) = \sum_{\vec{x}} \sum_{\vec{y}} \delta_{\vec{x} - \vec{y}, \vec{r}} \bar{d}_a(\vec{x}t) \gamma_5 u_a(\vec{x}t)$$

$$\times [\bar{d}_b(\vec{y}t) \gamma_5 \gamma_k d_b(\vec{y}t) + \bar{u}_b(\vec{y}t) \gamma_5 \gamma_k u_b(\vec{y}t)], \quad (10)$$

where $k = 1, 2, 3$. The relative distance $\vec{r}$ may in principle be used to construct operators that transform according to an irreducible representation of the hypercubic group. However, the simplest choice $\vec{r} = \vec{0}$ already leads to a viable operator. Summing over all spatial directions we thus adopt

$$O_{\pi a_1}(t) = \sum_{k=1}^{3} O_{\pi^+ a_1^0; k, \vec{0}}(t) \quad (11)$$
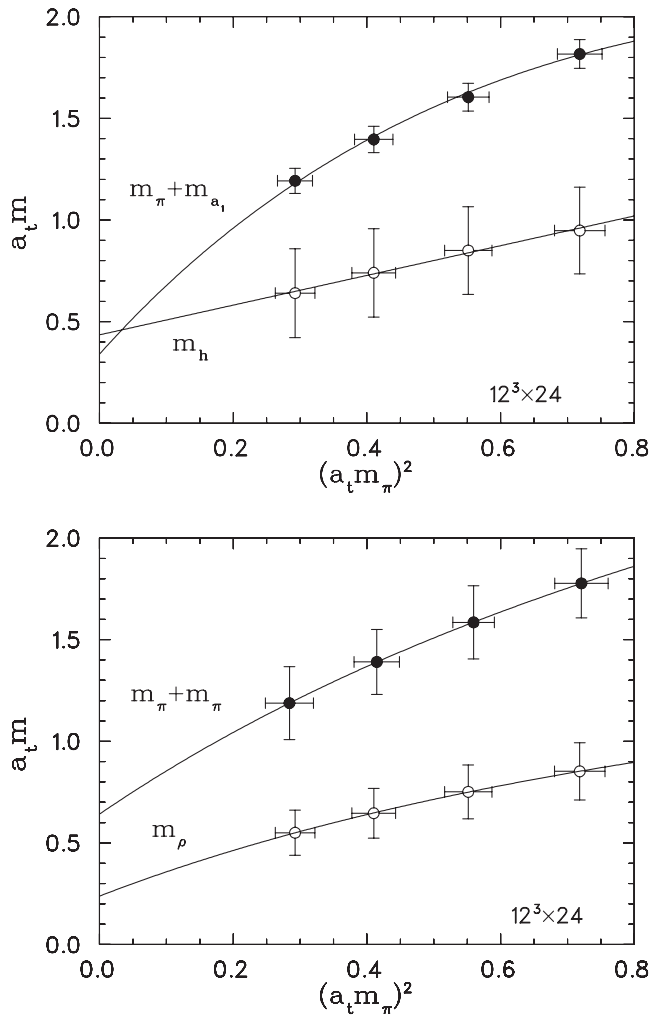
for this simulation.

FIG. 1. Combinations of masses, as indicated, obtained from single meson operators versus the squared pion mass $x = (a_t m_\pi)^2$ and fits with the model (9). The relative S-wave $\pi + a_1$ mass (upper panel) reveals a level crossing near zero pion mass through extrapolation. The $\pi + \pi$ mass is shown with pions having lattice momenta $\pm 2\pi/(a_s L)$. The extrapolation of the ρ meson mass to $x = 0$ is used to set the physical scale.

The operators (6) and (11) are the basis for calculating correlation functions

$$C_{XY}(t, t_0) = \langle O_X(t) O_Y^\dagger(t_0) \rangle - \langle O_X(t) \rangle \langle O_Y^\dagger(t_0) \rangle. \quad (12)$$

Here X and Y stand for h or πa_1, and thus establish a 2×2 correlation matrix. The separable terms in (12) are zero because of the quark flavor assignment in h and πa_1. The remaining (nonseparable) terms in (12) contain contractions between quark fields at equal times when worked out with Wick's theorem. For example, showing flavor structure only,

$$C_{h, \pi a_1}(t, t_0) \sim \langle (\bar{d}u)_t (\bar{d}d\bar{u}d + \bar{u}u\bar{u}d)_{t_0} \rangle \quad (13)$$

with time arguments t and t_0 as indicated. Equal-time contractions $:d\bar{d}:$ and $:u\bar{u}:$ occur only at the source time slice t_0. The corresponding propagator elements $Q^{-1}(\vec{x}t_0, \vec{y}t_0)$ are calculated by default. This is different for

$$C_{\pi a_1, \pi a_1}(t, t_0) \sim \langle (\bar{d}u\bar{d}d + \bar{d}u\bar{u}u)_t (\bar{d}d\bar{u}d + \bar{u}u\bar{u}d)_{t_0} \rangle, \quad (14)$$

where we encounter equal-time contractions $:d\bar{d}:$ and $:u\bar{u}:$ at $t > t_0$. The computation of $Q^{-1}(\vec{x}t, \vec{y}t)$ is very resource intensive and, if stochastic estimation is used [55], then it contributes additional noise.

We shall now argue that this problem can be circumvented: At $m_d = m_u$ the contractions $:d\bar{d}:$ and $:u\bar{u}:$ give rise to the same propagator elements $Q^{-1}(\vec{x}t, \vec{y}t)$. Thus, replacing the $(\ldots)_t$ term in (14) by $(2\bar{d}u\bar{d}d)_t$ and reinstating the γ-matrices from (10) we observe that $\bar{d}d \sim \bar{d}\gamma_5\gamma_k d$ couples to a_1 and f_1 mesons. Their masses are close however, 1230 MeV and 1282 MeV respectively [45]. Invoking a similar argument, altering the quark flavor $d \rightarrow s$ in the above operator entails $\bar{d}\gamma_5\gamma_k d \longrightarrow \bar{d}\gamma_5\gamma_k s \sim K_1$ and, again, should not significantly alter the mass spectra because the K_1 meson mass of 1270 MeV [45] again is close to that of the a_1 meson. In terms of (14) the effect is

$$C_{\pi a_1, \pi a_1}(t, t_0) \rightarrow \langle (2\bar{d}u\bar{d}s)_t (2\bar{s}d\bar{u}d)_{t_0} \rangle,$$

which now has no equal-time contractions, but otherwise is not different from (14) when worked out in terms of quark propagators. Hence, dropping equal-time contractions in (14) should have little effect on the mass spectrum of the πa_1 system, and ultimately, on the resulting decay width, because Lüscher's method for computing scattering phase shifts exclusively relies on the mass spectra, in a finite box.

We emphasize that the correlator element (14) is worked out using the quark flavor structure exactly as it emerges from (10) except that equal-time contractions are neglected. All other matrix elements are not effected.

Finally, we do not explicitly compute $C_{\pi a_1, h}(t, t_0)$ but rather infer it from the Hermicity of the correlation matrix.

IV. ANALYSIS

For every operator used in this simulation up to three iterations of quark field smearing [46] and gauge field fuzzing [47] were employed, using 2.5 as a strength parameter in both cases. The 2×2 correlation matrix (12) thus expands to size 6×6,

$$\mathcal{C}(t, t_0) = \begin{pmatrix} C_{h\{\}, h\{\}}(t, t_0) & C_{h\{\}, \pi a_1\{\}}(t, t_0) \\ C_{\pi a_1\{\}, h\{\}}(t, t_0) & C_{\pi a_1\{\}, \pi a_1\{\}}(t, t_0) \end{pmatrix}, \quad (15)$$

where the entries are 3×3 matrices with elements $C_{X\{k\}, Y\{\ell\}}(t, t_0)$ built from operators $O_{X\{k\}}(t, t_0)$, etc., with $k = 1, 2, 3$ levels of fuzzing and smearing. The latter is done identically at both source and sink, and thus the matrix $\mathcal{C}(t, t_0)$ is Hermitian by construction.

A standard analysis method is based on solving the generalized eigenvalue problem [38]

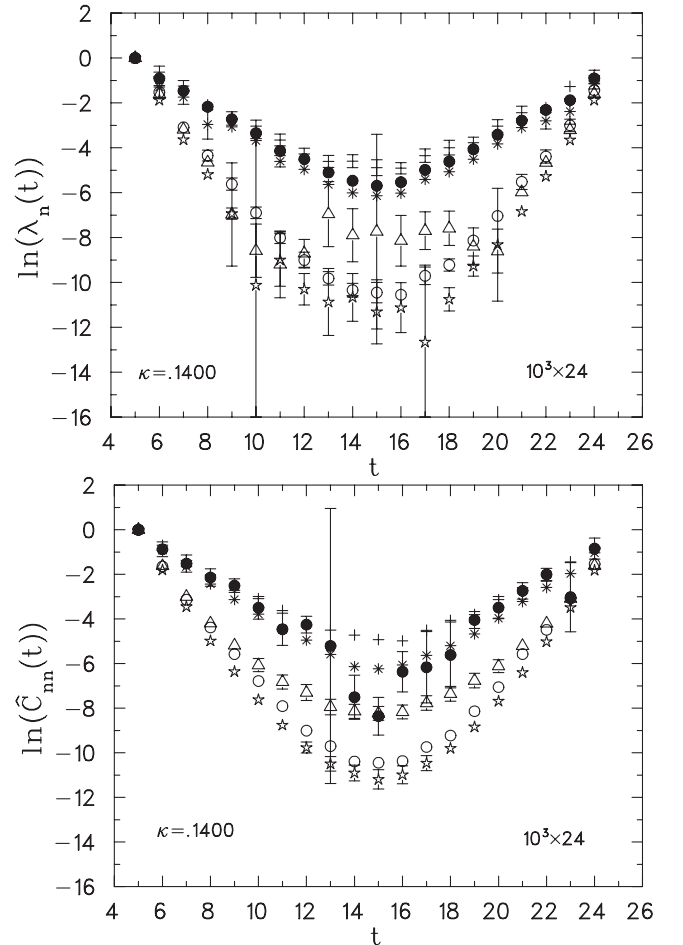$$\mathcal{C}(t, t_0)\Psi(t) = \mathcal{C}(t_1, t_0)\Psi(t)\Lambda(t), \quad (16)$$

FIG. 2. Comparison of eigenvalues obtained from diagonalizing $\hat{C}(t)$ on every time slice (upper panel) versus projecting to time slice $t = 5$ (lower panel), with $t_0 = 1$. Results are for the $10^3 \times 24$ lattice at the lightest pion mass. Fluctuations are much reduced using the projection technique.

where t_1 is fixed, $\Psi(t)$ is an $N \times N$ matrix, its columns being the generalized eigenvectors, and $\Lambda(t)$ is real diagonal. We further require that $\mathcal{C}(t_1, t_0)$ be positive definite. To ensure the latter t_1 should be an "early" time slice, here we use $t_1 - t_0 = 4$. The generalized eigenvalue problem (16) can then be cast into an ordinary one by first diagonalizing

$$\mathcal{C}(t_1, t_0) = V(t_1, t_0)D(t_1, t_0)V^{\dagger}(t_1, t_0), \qquad (17)$$

where $V(t_1, t_0)$ is unitary and $D(t_1, t_0)$ is real diagonal and positive definite. Inserting (17) into (16) we are lead to define

$$\hat{C}(t) = \frac{1}{\sqrt{D(t_1, t_0)}} V^{\dagger}(t_1, t_0)\mathcal{C}(t, t_0)V(t_1, t_0)\frac{1}{\sqrt{D(t_1, t_0)}}. \qquad (18)$$

Its eigenvalues are the same as those of the generalized problem (16), $\Lambda(t) = \text{diag}(\lambda_1(t) \ldots \lambda_N(t))$. Constructing $\hat{C}(t)$ merely amounts to a linear transformation among the set of operators $O_{X\{k\}}(t, t_0)$ that define the correlation matrix. Because of $\hat{C}(t_1) = \mathbb{1}$, the transformed set of operators create quantum states that are orthogonal and normalized at $t = t_1$. Provided that these match the "true" states of the theory, the eigenvectors of $\hat{C}(t)$ will stay orthogonal as $t \geq t_1$ increases to the extent allowed by the errors of the simulation. Consequently $\hat{C}(t)$ will be diagonal dominated for $t \geq t_1$.

From an analysis point of view there are now two options: One may diagonalize $\hat{C}(t)$ on each time slice t separately and thus obtain the eigenvalues $\lambda_n(t)$, $n = 1 \ldots N$, as proposed in [38]. Alternatively, the diagonal elements of $\hat{C}(t)$ may be taken as an approximation to its eigenvalues,

$$\lambda_n(t) \approx \hat{C}_{nn}(t), \qquad n = 1 \ldots N, \qquad (19)$$

which involves projecting $\hat{C}(t)$ into the eigenspaces at fixed time slice t_1, see (18). The latter approach has the advantage that statistical fluctuations are reduced, see Fig. 2 for a comparison. This is plausible because fluctuations of the eigenvector components are effectively frozen. It also has the advantage to tag the eigenvalues to a specific eigenvector, which is important for tracking the quark mass dependence of the spectral levels.

Effective mass function plateaus typically develop in the time interval $5 \lesssim t - t_0 \lesssim 10$, or so. In this region the projection technique yields more stable results, particularly for the excited states. An example for the $12^3 \times 24$ lattice at $\kappa = 0.140$ is shown in Fig. 3.

Thus we will continue our analysis with the projected correlators and, for simplicity, refer to $\hat{C}_{nn}(t)$ as eigenvalues $\lambda_n(t)$. Those then give rise to the spectral energies W_n, $n = 1 \ldots 6$, listed in Table II.

Fits to those spectra with the model (9) are shown in Fig. 4. This figure sheds light on the volume dependence of the spectral levels. Evidently the ground state mass is
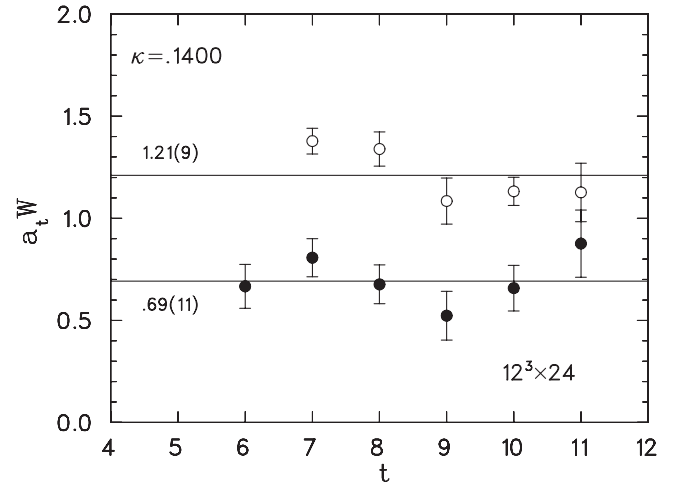

FIG. 3. Example of effective mass functions for two (projected) eigenvalues of the correlation matrix $\hat{C}(t)$ on the $12^3 \times 24$ lattice at the lightest pion mass. The higher mass comes from $\lambda_5(t)$ and the lower mass from $\lambda_2(t)$.

relatively stable against changing the lattice volume. On the other hand the effect on excited states is clearly significant, even to the extent that level crossing patterns differ for some of the states. This should not be surprising because excited levels are likely to describe two-meson states, which are spatially large. Nevertheless, anticipating results, the volume effect on the scattering phase shift ultimately turns out to be only moderate.

Another comment on Fig. 4 is that, although the 6×6 correlation matrix gives rise to six eigenvalues, the number of physical states on the lattice is likely to be a lesser number because, typically, hadronic level spacings are of the order of a few hundred MeV. Thus we entertain the possibility that the group of the three lower levels in Fig. 4 describe the same state, the ground state, whereas the upper levels belong to two-meson states with some degree of

TABLE II. Energy spectra W_n, $n = 1 \ldots 6$ from the $12^3 \times 24$ lattice (upper table) and the $10^3 \times 24$ lattice (lower table) at four pion masses.

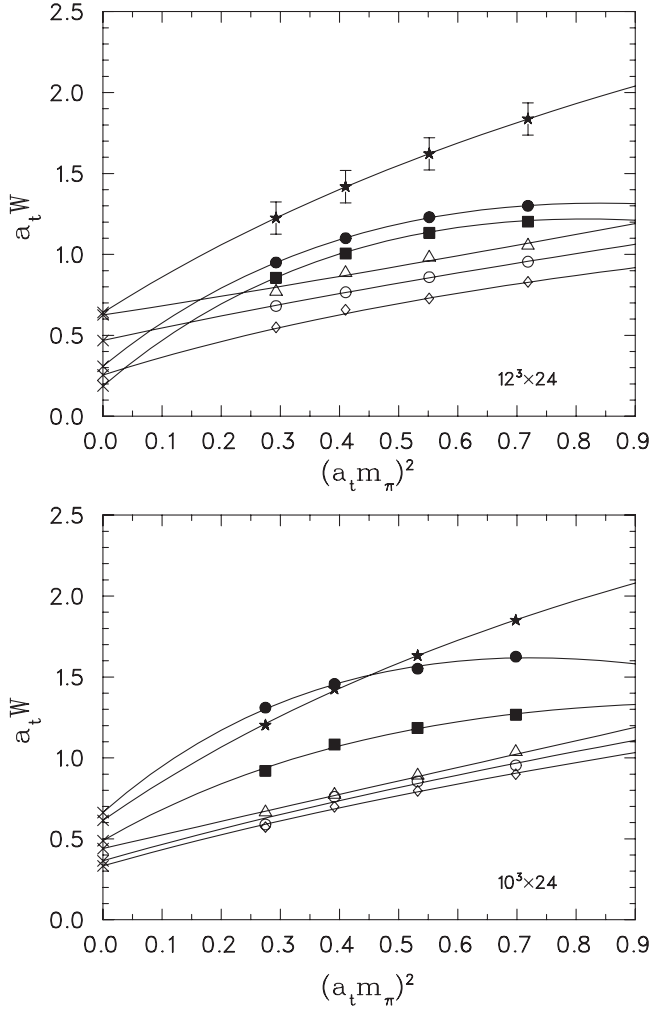| κ	0.140	0.136	0.132	0.128
$a_t W_1$	0.55(14)	0.69(2)	0.74(4)	0.82(10)
$a_t W_2$	0.69(11)	0.79(3)	0.89(4)	0.93(9)
$a_t W_3$	0.81(10)	0.81(4)	0.91(4)	1.03(7)
$a_t W_4$	0.88(13)	1.03(11)	1.18(10)	1.26(5)
$a_t W_5$	1.21(9)	1.13(3)	1.25(3)	1.31(4)
$a_t W_6$	0.96(5)	1.42(4)	1.62(3)	1.85(4)
$a_t W_1$	0.57(7)	0.69(11)	0.75(11)	0.78(6)
$a_t W_2$	0.59(11)	0.71(5)	0.78(4)	0.81(5)
$a_t W_3$	0.61(6)	0.74(5)	0.80(4)	0.91(5)
$a_t W_4$	0.91(11)	1.12(8)	1.14(13)	1.24(9)
$a_t W_5$	1.20(9)	1.42(11)	1.64(9)	1.78(9)
$a_t W_6$	1.31(6)	1.43(6)	1.55(9)	1.62(13)

FIG. 4.   Mass spectra obtained from the $12^3 \times 24$ and $10^3 \times 24$ lattices versus $x = (a_t m_\pi)^2$. Error bars are omitted for clarity except for one level where the errors shown are typical of all levels. Fits with the model (9) are shown as lines.

interaction energy due to their relative motion. This point will become more plausible in terms of the corresponding scattering phase shifts.

V. SCATTERING PHASE SHIFTS

The spectral energies W_n computed on the lattice give rise to a discrete set of relative $\pi + a_1$ momenta k_n by solving the relativistic dispersion relation

$$W_n = \sqrt{m_\pi^2 + k_n^2} + \sqrt{m_{a_1}^2 + k_n^2}. \qquad (20)$$

Note that the resulting momenta k_n relate to spectral masses and thus are continuous numbers (not subject to lattice discretization). Only those levels W_n will be used that fall within the elastic region,

$$(m_\pi + m_{a_1}) < W_n < 2(m_\pi + m_{a_1}). \qquad (21)$$

Continuum S-wave scattering phase shifts $\delta_0(k)$ are then

computed at a discrete set of momenta k_n using Lüscher's formula [19],

$$\tan\delta_0(k_n) = -\frac{\pi^{3/2} q_n}{\mathcal{Z}(1; q_n^2)}, \qquad q_n = \frac{k_n L_s}{2\pi}. \qquad (22)$$

Here $\mathcal{Z}(1; q^2)$ is a generalized ζ-function, and $L_s = L a_s$ is the physical size of the spatial box, using the bare anisotropy $a_s = 2a_t$.

If the number of available data points is sufficient, then one may attempt a fit to a Breit-Wigner function [56],

$$\tan\delta_0(k) = \frac{\Gamma/2}{E_0 - W(k)} \qquad (23)$$

where $W(k) = \sqrt{m_\pi^2 + k^2} + \sqrt{m_{a_1}^2 + k^2}. \qquad (24)$

The resonance energy E_0 and the decay width Γ are fit parameters. However, a successful fit can only be expected if the underlying physics indeed supports an isolated resonance. Such a fit actually fails for all spectra computed at the four pion masses, or rather $x = (a_t m_\pi)^2$, as they appear in Fig. 4. This is not be surprising because those data points are far away from a level crossing between the h and the $\pi + a_1$ masses as evident from Fig. 1. It is necessary to extrapolate the spectral masses to $x = 0$ near the level crossing. The model (9) has been used for this purpose. We present the extrapolated spectra in Table III along with the corresponding momenta k_n and scattering phase shifts $\delta_0(k_n)$ for those levels which fall into the elastic region (21).

The phase shift data are very sparse and do not alone resolve the functional form of the fit model, such as Breit-Wigner. In fact, attempts of Levenberg-Marquardt fits us-

TABLE III.   Extrapolated energy spectra W_n using the model (9), resulting momenta k_n, and S-wave scattering phase shifts on lattices $12^3 \times 24$ (upper table) and $10^3 \times 24$ (lower table). Missing entries for $a_t k_n$ and $\delta_0(k_n)$ correspond to energy levels outside of the elastic region (21).

n	$a_t W_n$	$a_t k_n$	$\delta_0(k_n)$
1	0.64(16)	0.16(1)	74.6(11.6)
2	0.63(25)	0.15(2)	65.8(14.1)
3	0.19(5)	$\cdots$	$\cdots$
4	0.47(11)	0.03(1)	2.1(1.8)
5	0.31(11)	$\cdots$	$\cdots$
6	0.26(5)	$\cdots$	$\cdots$
1	0.66(21)	0.20(2)	77.1(10.5)
2	0.61(3)	0.16(1)	50.0(6.1)
3	0.49(4)	0.06(1)	6.0(3.1)
4	0.44(10)	0.01(1)	0.2(0.5)
5	0.36(10)	$\cdots$	$\cdots$
6	0.33(4)	$\cdots$	$\cdots$

TABLE IV. Results for decay widths Γ and resonant energies E_0 for two lattice sizes L in units of a_t, and with a physical scale set by the ρ meson mass.

L	$a_t\Gamma$	a_tE_0	Γ [MeV]	E_0 [GeV]
12	0.012(9)	0.63(3)	35(26)	1.88(8)
10	0.032(14)	0.62(3)	97(43)	1.84(9)

ing (23) only returned stable results for the resonance energy parameter a_tE_0, while the width parameter $a_t\Gamma$, being an indicator for a derivative, was left undetermined due to large standard errors. Nevertheless, it is evident from Table III that the phase shift data are clustered around two regions of a_tk_n, namely $\approx$ 0.15–0.16 and $\approx$ 0.03 for the $L = 12$ lattice, and $\approx$ 0.16–0.20 and $\approx$ 0.01–0.06 for the $L = 10$ lattice. This suggests that no more than two distinct physical states are uncovered by the simulation. Under this assumption the data may be analyzed as follows: Denoting the weighted ($\chi^2 = $ min) averages for each of the clustered momenta by $\bar{k}_{1,2}$, the corresponding energies by $\omega_{1,2} = a_tW(\bar{k}_{1,2})$, and $\tau_{1,2} = \tan\delta_0(\bar{k}_{1,2})$, we obtain a set of two equations from (23), for each lattice, which are solved exactly by

$$a_t\Gamma = 2(\omega_1 - \omega_2)\frac{\tau_1\tau_2}{\tau_1 + \tau_2} \qquad (25)$$

$$a_tE_0 = \frac{\omega_2\tau_2 - \omega_1\tau_1}{\tau_2 - \tau_1}. \qquad (26)$$

The resulting parameter values are listed in Table IV. There, the uncertainties for $a_t\Gamma$ and a_tE_0 are computed as follows: The statistical (jackknife) errors for a_tk_n, as they appear in Table III, give rise to errors $\triangle\bar{k}_{1,2}$ for the weighted momentum averages $\bar{k}_{1,2}$. Repeating the analysis procedure described above a few thousand times with momenta $k_{1,2} = \bar{k}_{1,2} + \xi\Delta\bar{k}_{1,2}$, where ξ is a normal distributed random deviate with variance one, then yields the uncertainties given in Table IV. Also the a_1 meson mass, which enters the fit model via (24), was subjected to the same randomization. The errors given in Table IV are the standard deviations resulting from the randomization, they are reminiscent of statistical errors. Table IV also contains the physical values for the decay widths and the resonance energies using the ρ meson to set the mass scale. Setting the scale with the a_1 meson mass, results in widths of 39(29) MeV and 108(48) MeV for the $12^3 \times 24$ and $10^3 \times 24$ lattices, respectively.

Finally, Fig. 5 shows the combined phase shift data from the two lattices on a common physical scale. The curves are Breit-Wigner interpolations as explained above.

VI. ERRORS

All errors cited in this paper are statistical, and are derived from a standard jackknife procedure [57]. The hybrid meson operator, involving gauge link paths, appears to be the major source of those.

The effects of systematic errors on the results of this simulation are difficult to assess. In principle this can only be done by repeating it with various different choices of lattice and analysis model parameters. Probably the largest sources of systematic error stem from curve fitting and extrapolation techniques. As a check on the extrapolations we have also done fits with a $x^{3/2}$ term in place of the logarithmic term in (9). The results, Table IV, did not change much, within statistical errors. If only linear terms are retained the extrapolated masses slightly shift upward, ultimately resulting in a slight increase of decay widths on the order of $\approx$ 10 MeV.

Another source of systematic error comes from postulating a Breit-Wigner model. Given the sparsity of data points it is inconclusive that the physical phase shifts will indeed follow a Breit-Wigner form. In order to resolve this problem the simulation would have to be repeated at several values of the gauge coupling β, thus mapping out some sort of continuous curve $\delta_0(k)$ vs k. The results of this work do rely on the *a priori* assumption that the simulation data follow a Breit-Wigner model.
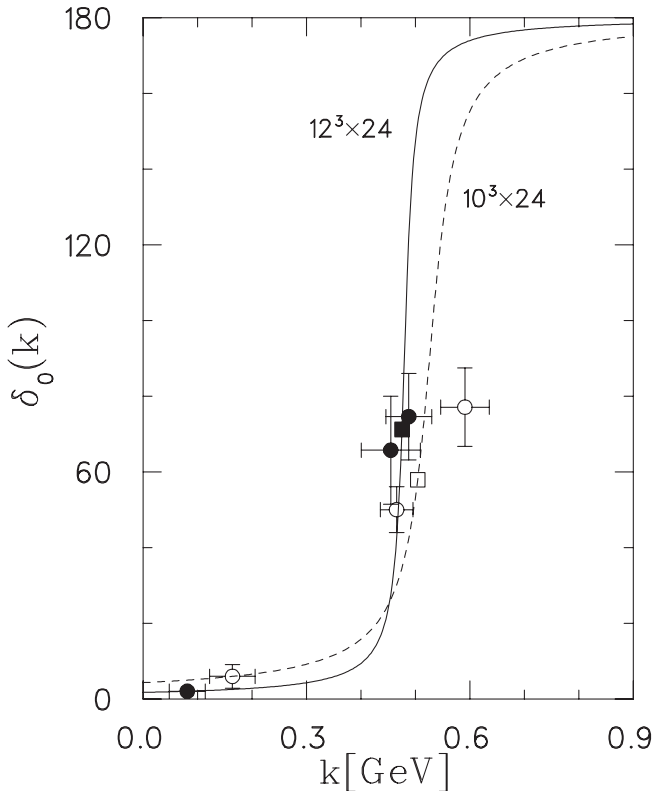

FIG. 5. Scattering phase shifts $\delta_0(k_n)$ from the lattices $12^3 \times 24$ (filled circles) and $10^3 \times 24$ (open circles). The solid and dashed curves are Breit-Wigner interpolations according to (25) and (26). The filled and open box plot symbols indicate the respective χ^2-weighted averages over data points.

On the other hand, adopting the less stringent criterion that a resonance is present if the phase shift data passes through 90°, the simulation results clearly indicate the presence of such. This, in itself, is a significant outcome of this project. Although this does not help putting bounds on the systematic error of Γ, the results for the resonance energy, $E_0 \approx 1.9$ GeV, are remarkably stable. A decay width, on the other hand, essentially comes from derivative data and as such is prone to a significantly larger error.

Systematic errors are also caused by finite size effects. At first sight, judging by the small difference of the ρ meson masses on the $L = 12$ and $L = 10$ lattices, see Table I, those appear to be small. Finite size effects should be expected to be much larger for larger-sized hadrons like the a_1 for example. This is particularly true for two-hadron systems studied in this work. For example, the spectra displayed in Fig. 4 are significantly different, particularly for excited states on the $L = 12$ and $L = 10$ lattices, their size though being quite similar. Again these effects can only be studied by repeating this simulation with several lattices of different sizes.

Obtaining a single scattering phase data point requires evaluating up to three effective mass functions—one for the correlator matrix eigenvalue, one for the ρ meson to set the physical scale, and one for the π meson. The variability in choosing which time slices of the correlation functions to use in fitting effective masses produces a variability in the decay width. Here, one usually wants to maximize the plateau width of the effective mass functions to optimize the statistical error. Reducing the plateau width to estimate a systematic error is of limited value.

VII. CONCLUSION

Decay widths for the hybrid exotic meson with $J^{PC} = 1^{-+}$, calculated using Lüscher's method, are in the range 35 to 97 MeV with statistical errors of about 30 MeV using the ρ meson to set the scale. The lower value for the width came from using extrapolated energy spectra on a $12^3 \times 24$ lattice and the higher value came from using extrapolated spectra on a $10^3 \times 24$ lattice. If the a_1 meson sets the scale, then the widths for these two lattices range from 39 to 108 MeV with statistical errors of about 40 MeV.

The number of data points available to fit Breit-Wigner functions is very sparse, the reason being that many energy levels fell outside the elastic region where phase shifts using Lüscher's formulas cannot be computed. Overcoming this limitation requires use of a larger correlation matrix. This can be accomplished by adding more smearing levels, and spatially extended operators in the individual correlators, or possibly by using a coupled channel type analysis in which more than one decay channel is represented in the matrix. Several values of the coupling parameter β should also be employed to generate more phase shift data points.

Using the ρ meson to set the scale, the resonance mass of the hybrid meson in this simulation was 1.9(1) GeV, and in contrast to the decay width, the resonance mass was well determined by the simulation. This unexpected result leads to a final comment that, historically, hadron mass calculations within lattice QCD have been done using single-hadron operators, ignoring the fact that most hadrons are resonances and thus are unstable [17]. We have taken this decay aspect seriously. Although the numerical values for the decay widths serve as a guide only, the approach of extracting hadron masses as resonance energies, using Lüscher's method, should also be given serious consideration.

[1] T. Barnes, nucl-th/0303032.
[2] T. Barnes, nucl-th/0009011.
[3] T. Barnes, Acta Phys. Pol. B **31**, 2745 (2000).
[4] D. Alde *et al.* (IHEP-Brussels-Los Alamos-Annecy (LAPP)), Phys. Lett. B **205**, 397 (1988).
[5] D. R. Thompson *et al.* (E852), Phys. Rev. Lett. **79**, 1630 (1997).
[6] A. Abele *et al.* (Crystal Barrel), Phys. Lett. B **423**, 175 (1998).
[7] G. S. Adams *et al.* (E852), Phys. Rev. Lett. **81**, 5760 (1998).
[8] S. U. Chung *et al.* (E852), Phys. Rev. D **60**, 092001 (1999).
[9] E. I. Ivanov *et al.* (E852), Phys. Rev. Lett. **86**, 3977 (2001).
[10] A. R. Dzierba *et al.*, Phys. Rev. D **73**, 072001 (2006).
[11] T. Barnes, F. E. Close, F. de Viron, and J. Weyers, Nucl. Phys. **B224**, 241 (1983).
[12] T. Barnes, F. E. Close, and E. S. Swanson, Phys. Rev. D **52**, 5242 (1995).
[13] F. E. Close and P. R. Page, Nucl. Phys. **B443**, 233 (1995).
[14] C. McNeile and C. Michael (UKQCD), Phys. Rev. D **73**, 074506 (2006).
[15] C. McNeile, C. Michael, and P. Pennanen (UKQCD), Phys. Rev. D **65**, 094505 (2002).
[16] C. Michael, Nucl. Phys. **B327**, 515 (1989).
[17] C. Michael, PoS, LAT2005 (2005) 008.
[18] T. A. DeGrand, Phys. Rev. D **43**, 2296 (1991).
[19] M. Lüscher, Nucl. Phys. **B364**, 237 (1991).

[20] L. Lellouch and M. Lüscher, Commun. Math. Phys. **219**, 31 (2001).
[21] K. J. Juge, J. Kuti, and C. J. Morningstar, Phys. Rev. Lett. **82**, 4400 (1999).
[22] K. J. Juge, J. Kuti, and C. J. Morningstar, Nucl. Phys. B, Proc. Suppl. **63**, 326 (1998).
[23] S. Perantonis and C. Michael, Nucl. Phys. **B347**, 854 (1990).
[24] T. Burch, K. Orginos, and D. Toussaint, Phys. Rev. D **64**, 074505 (2001).
[25] I. T. Drummond, N. A. Goodman, R. R. Horgan, H. P. Shanahan, and L. C. Storoni, Phys. Lett. B **478**, 151 (2000).
[26] T. Manke, I. T. Drummond, R. R. Horgan, and H. P. Shanahan (UKQCD), Nucl. Phys. B, Proc. Suppl. **63**, 332 (1998).
[27] C. McNeile *et al.*, Nucl. Phys. B, Proc. Suppl. **73**, 264 (1999).
[28] C. W. Bernard *et al.* (MILC), Phys. Rev. D **56**, 7039 (1997).
[29] C. W. Bernard *et al.*, Nucl. Phys. B, Proc. Suppl. **53**, 228 (1997).
[30] P. Lacock and K. Schilling (TXL), Nucl. Phys. B, Proc. Suppl. **73**, 261 (1999).
[31] P. Lacock, C. Michael, P. Boyle, and P. Rowland (UKQCD), Nucl. Phys. B, Proc. Suppl. **63**, 203 (1998).
[32] P. Lacock, C. Michael, P. Boyle, and P. Rowland (UKQCD), Phys. Lett. B **401**, 308 (1997).
[33] P. Lacock, C. Michael, P. Boyle, and P. Rowland (UKQCD), Phys. Rev. D **54**, 6997 (1996).
[34] C. Bernard *et al.* (MILC), Nucl. Phys. B, Proc. Suppl. **119**, 260 (2003).
[35] C. McNeile and C. Michael (UKQCD), Phys. Lett. B **556**, 177 (2003).
[36] M. Lüscher, Nucl. Phys. **B354**, 531 (1991).
[37] M. S. Cook, *Exotic Meson Decay Widths using Lattice Quantum Chromodynamics* (Florida International University, Miami, Florida, 2006).
[38] M. Lüscher and U. Wolff, Nucl. Phys. **B339**, 222 (1990).
[39] M. Göckeler, H. A. Kastrup, J. Westphalen, and F. Zimmermann, Nucl. Phys. **B425**, 413 (1994).
[40] F. Zimmermann, J. Westphalen, M. Göckeler, and H. A. Kastrup, Nucl. Phys. B, Proc. Suppl. **30**, 879 (1993).
[41] H. R. Fiebig, A. Dominguez, and R. M. Woloshyn, Nucl. Phys. **B418**, 649 (1994).
[42] C. R. Gattringer and C. B. Lang, Nucl. Phys. **B391**, 463 (1993).
[43] C. R. Gattringer, I. Hip, and C. B. Lang, Nucl. Phys. B, Proc. Suppl. **30**, 875 (1993).
[44] R. D. Loft and T. A. DeGrand, Phys. Rev. D **39**, 2692 (1989).
[45] S. Eidelman *et al.*, Phys. Lett. B **592**, 1 (2004).
[46] C. Alexandrou, S. Güsken, F. Jegerlehner, K. Schilling, and R. Sommer, Nucl. Phys. **B414**, 815 (1994).
[47] C. Albanese *et al.*, Phys. Lett. B **192**, 163 (1987).
[48] C. Bernard *et al.*, Phys. Rev. D **56**, 7039 (1997).
[49] A. Frommer, B. Nöckel, S. Güsken, T. Lippert, and K. Schilling, Int. J. Mod. Phys. C **6**, 627 (1995).
[50] *Chiral Dynamics: Theory and Experiment*, edited by A. M. Bernstein and B. R. Holstein, Lecture Notes in Physics vol. 452 (Springer-Verlag, Berlin, Heidelberg, New York, 1995).
[51] A. Thomas and A. Szczepaniak, Phys. Lett. B **526**, 72 (2002).
[52] J. Smit, *Introduction to Quantum Fields on a Lattice* (Cambridge University Press, Cambridge, UK, 2002).
[53] S. V. Wright *et al.*, Nucl. Phys. B, Proc. Suppl. **109**, 50 (2002).
[54] J. N. Hedditch *et al.*, Phys. Rev. D **72**, 114507 (2005).
[55] C. Michael and J. Peisa (UKQCD), Phys. Rev. D **58**, 034506 (1998).
[56] J. R. Taylor, *Scattering Theory* (Wiley, New York, 1972).
[57] B. Efron, SIAM Rev. **21**, 460 (1979).